

## **CHAPTER 2: COMPUTER MODELING**

### **2.1 Assumptions**

Several assumptions were made when modeling the geotextile tube. These include: the geotextile had a small amount of bending stiffness; the thickness of the geotextile was 3mm (Koerner 1994); the geotextile was impermeable; the geotextile was linearly elastic with a Young's modulus of  $7.0346 \times 10^9$  Pa; Poisson's ratio for the geotextile was 0.45; the geotextile had a density of  $75.0 \text{ kg/m}^3$  (Veldhuijzen van Zanten 1986); the springs used to model the elastic foundation were only active in the vertical direction; compression springs had a constant stiffness; the specific weight of the slurry was 1.5 times that of water; and the tube was symmetric about both the XZ plane and the YZ plane. The directions of the X-, Y-, and Z-axes are described in the Nomenclature section of this thesis.

### **2.2 Using ABAQUS as a Finite Element Program**

#### **2.2.1 Introduction**

A geotextile tube was modeled using the commercial finite element analysis program ABAQUS (Hibbitt, et al. 1994). In this chapter, nonlinear geometric analysis is discussed; the geotextile tube was modeled using this type of analysis. Next, the various types of shell and spring elements available in ABAQUS are presented, along with an explanation of why the S4R and SPRING1 elements were chosen to model the top and bottom surfaces of the geotextile tube and the elastic foundation, respectively. The manner in which the elements were used to construct the model are not discussed in detail until Section 2.3; Section 2.2 is meant to provide the reader with background information needed to better understand the model when it is described in detail in Section 2.3.

### **2.2.2 Nonlinear Analysis**

A geometrically nonlinear analysis was performed on the geotextile tube model. This type of analysis takes large displacements into account; it does not linearize kinematic relationships like linear analyses do. At each load increment, equilibrium is satisfied based upon the model's current configuration, not the original one. Load increments should be kept small.

### **2.2.3 Hydrostatic Pressure**

Hydrostatic pressure was applied to the geotextile tube to model the pumped slurry. The hydrostatic pressure was assumed to have a specific weight of 1.5 times that of water. The hydrostatic pressure was added in increments in such a way that the pressure head was constant throughout the analysis, and the density was increased at each increment until it reached the density of the slurry. At this point, the state of the structure was analyzed.

### **2.2.4 Elements**

#### **2.2.4.1 Shell**

When choosing an element to model the geotextile, membrane elements were considered. Membranes only act in tension. It is very possible for a geotextile tube to have some wrinkling in the material once it is pumped full of slurry, especially since its initial shape is a flat rectangle. When wrinkling occurs, there is both compression and tension in the model. Because a membrane element would likely have problems modeling a tube with wrinkling, shell elements were used instead to model the geotextile.

There are many different shell elements in ABAQUS, each of which is placed in one of three categories: general-purpose shells (S3R, S4R), thick shells (S8R, S8RT), and thin shells (STRI3, STRI35, S4R5, STRI65, S8R5, S9R5). General-purpose shells are capable of deformation due to transverse shear stress. Thin shells should be used only if transverse shear deformation is negligible; in this case, the elements satisfy the Kirchhoff assumption throughout the analysis. Thick shells take transverse shear deformation into account and should be used when this deformation is important in the model. Initially, it was uncertain whether or not shear deformation was going to be important.

Finite-strain elements (S3R, S4R) allow the element thickness to change during the analysis. The thicknesses of small-strain elements (STRI3, STRI35, S4R5, STRI65, S8R, S8RT, S8R5, S9R5) do not change during analysis. In order to obtain a fully non-linear model, finite-strain elements must be used. When bending occurs in a thin shell, curved elements (STRI35, STRI65, S3R, and S4R) are recommended. For these reasons, the doubly-curved element S4R was chosen to model the geotextile tube.

The S4R element is a four-node element. Each node has three displacement and three rotation degrees of freedom. Each of the six degrees of freedom uses an independent bilinear interpolation function.

The S4R element uses a mixed finite element formulation; in this formulation, neither pure Kirchhoff nor pure Mindlin theory is used. Instead, thick shells use a theory similar to that of Mindlin and the formulation of thin shells is similar to that of the discrete Kirchhoff theory. A transverse shear strain field is used in the formulation and is discussed in detail in the ABAQUS Theory Manual. The transverse shear formulation of the S4R element is similar to that of the Bathe-Dvorkin plate element (Hibbitt, et al. 1994).

The S4R element is a reduced integration element. Reduced integration elements converge nonmonotonically, whereas elements which do not have reduced integration

converge monotonically. Reduced integration reduces the amount of CPU time necessary for analysis of the model, and it typically provides results which are more accurate. Due to the reduced number of integration points, hourglassing can occur in the S4R element. An hourglass stabilization control feature is built into the element; therefore, ABAQUS automatically checks for the possible hourglass mode shapes.

### 2.2.4.2 Spring

Springs were used to model the elastic foundation. They were modeled as tensionless springs such that when in compression, they are active, and when in tension, they are inactive and uplift occurs. Figure 2.2.4.2.1 demonstrates how a spring with a stiffness of 10,000 N/m is modeled in ABAQUS. If there is negative deflection, each spring has a stiffness of 10,000 N/m, which is the slope of the line in the figure, and for zero or positive deflection, each spring has a stiffness of zero.

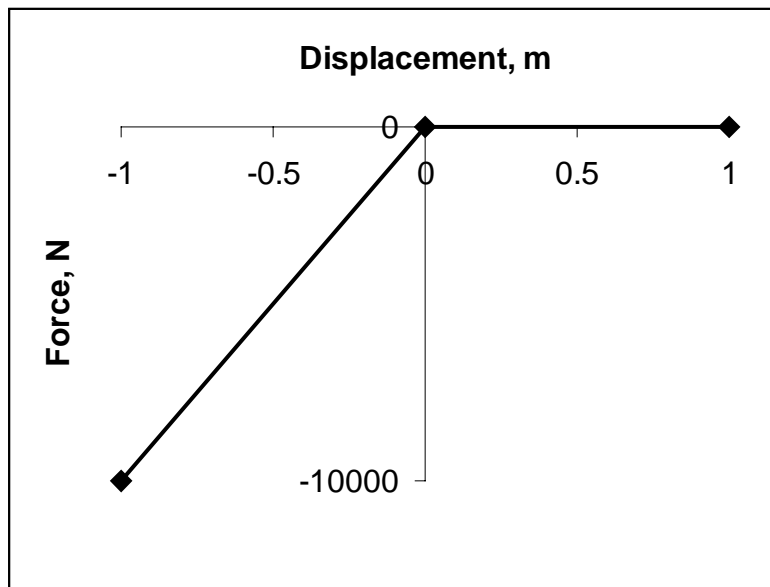


Figure 2.2.4.2.1: Stiffness of a Tensionless Spring

SPRING1 elements were used to model the elastic foundation in the model. This type of element has one end attached to the ground, i.e., a rigid surface, and the other end

attached to a node in the model. The spring provides stiffness to a global degree of freedom. This type of spring does not rotate with large displacement analysis.

An iteration procedure was performed on an example to check that the springs were inactive when in tension. A simplified three-dimensional model of the tube was constructed, resting on an elastic foundation. Each spring which made up the elastic foundation had a stiffness of 10,000 N/m when both in tension and compression. Hydrostatic pressure was applied to the model. Those springs which were in tension were removed. Hydrostatic pressure was then applied to the new model and again springs which were in tension were removed. This iteration procedure continued until convergence occurred. The results obtained (the contact region and the deflections) from this final iteration were the same as those obtained from a tube modeled the same way but resting on tensionless springs. Therefore, the tensionless springs were working as expected and desired.

## **2.3 Models**

### **2.3.1 Introduction**

Several tubes were modeled, having different initial shapes. Changes were continuously made to the initial shape until convergence difficulties were overcome. This section discusses the changes that were made to the initial model and then explains the final model in detail.

### **2.3.2 Initial Models Which Led to the Final Model**

The initial shape studied consisted of two flat rectangles, each 3.0m x 1.5m, made up of S4R shell elements. Twenty elements were used to model the 1.5m width, and 40 were used to model the length; therefore, each rectangle consisted of 800 elements. Constraints were applied to the model such that corresponding nodes at the edges had the same X-, Y-, and Z-translations. These constraints were used to model the way the

geotextile sheets are typically sewn together at their edges. Each node on the bottom surface had a spring attached to it. The other end of the spring was attached to the ground. Each spring had a stiffness of 40,000 N/m when in compression and 0 N/m when in tension. The springs provided stiffness in the direction of the global Z-axis (vertical direction). This model is shown in Figure 2.3.2.1. The elastic foundation is not shown in the figures.

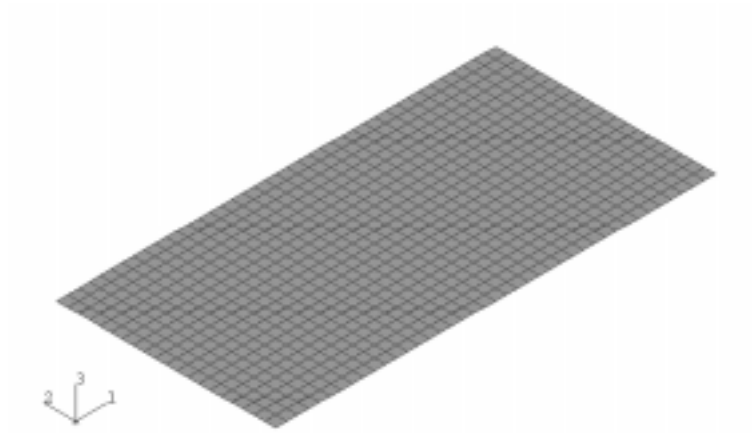


Figure 2.3.2.1: Original Model

The model had convergence difficulties. The tensionless springs were thought to be the problem; therefore, the model was changed so that each spring would have a stiffness of 40,000 N/m whether in compression or tension. To make the springs behave only in compression, the aforementioned iteration procedure was going to be used. This change to the model improved convergence, but not completely. The mesh was then refined so that there were 40 elements across the width and 80 along the length. Ironically, this made convergence worse.

Another possible cause of the difficulties was that too many constraints were being placed on the nodes along the edges. The model was then changed so that the two 3.0m x 1.5m rectangles, made up of S4R elements, had the same node numbers at the

edges. Therefore, the deflection constraints did not need to be applied to the edge nodes because there was only one set of edge nodes. This change to the model did improve convergence, but not completely.

Because shell elements were used and the model was initially flat, when hydrostatic pressure was applied to the model, the edges came together to a point, as shown in Figure 2.3.2.2. Geotextile tubes are smooth at the edges; they do not have discontinuous slopes at the edges. To overcome this problem and to hopefully improve convergence, further changes were made to the model.

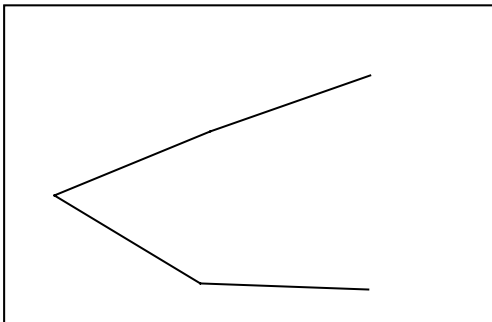


Figure 2.3.2.2: Cross Section of Edge, Which Was Initially Flat

A two-foot-long piece of rubber with a thickness of 2mm was folded (or "flipped") over to obtain the shape shown in Figure 2.3.2.3. A new model was constructed with its initial shape having edges with the exact same shape as the curve shown in the figure. One-quarter of the tube was modeled with the new edges, and its initial shape is shown in Figure 2.3.2.4. A close-up of the edges is shown in Figure 2.3.2.5. Tensionless springs were connected to each node on the bottom surface and had a spring stiffness of 5700 N/m. This model was more refined than the previous model discussed. In a one-quarter model, 15 elements made up the half-width of the surfaces and 30 made up the half-length. Thirty-one elements were used to model the cross section of the "flipped" edges. Because shell elements were used in this model, when

hydrostatic pressure was applied, the top portion of the "flipped" edges had trouble opening up. This is shown in Figure 2.3.2.6. The edges needed to be modified further.

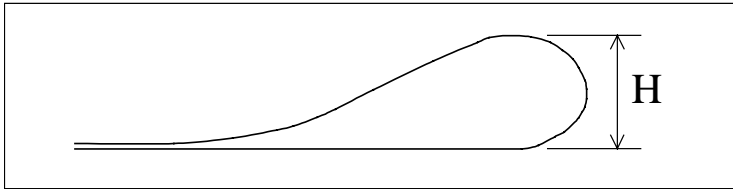


Figure 2.3.2.3: Cross Section of "Flipped" Edge; Height,  $H = 0.0429\text{m}$

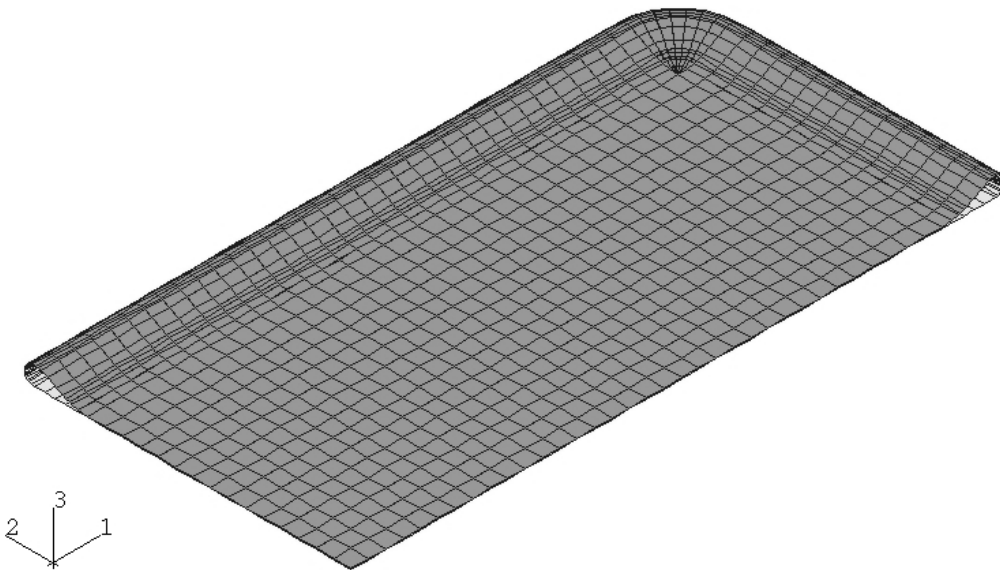


Figure 2.3.2.4: Initial Shape of One-Quarter Model with "Flipped" Edges

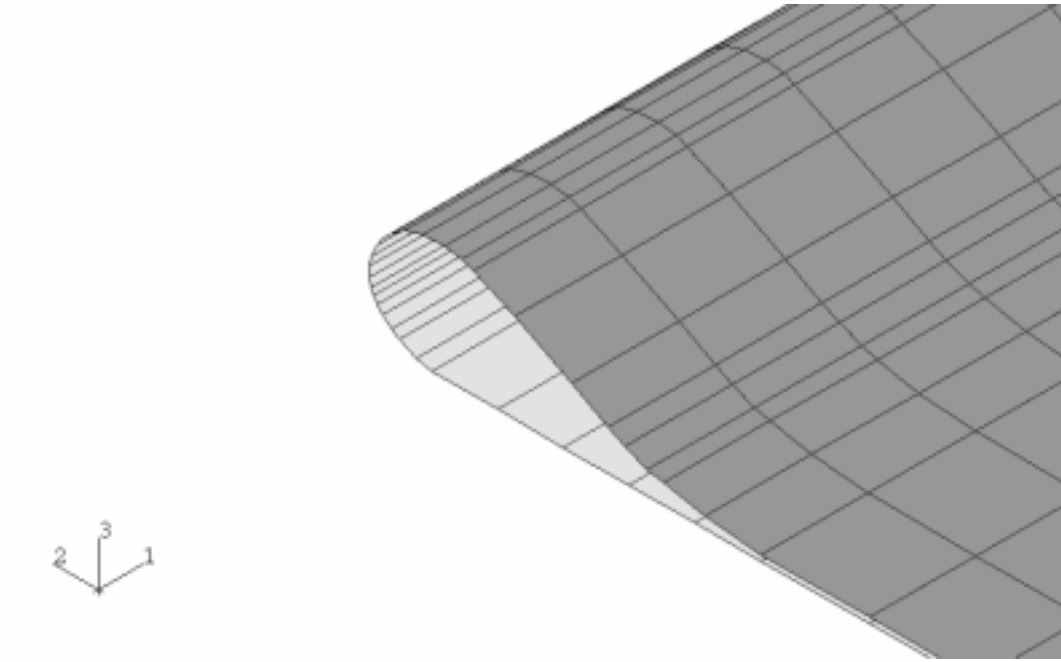


Figure 2.3.2.5: Close-Up of "Flipped" Edges

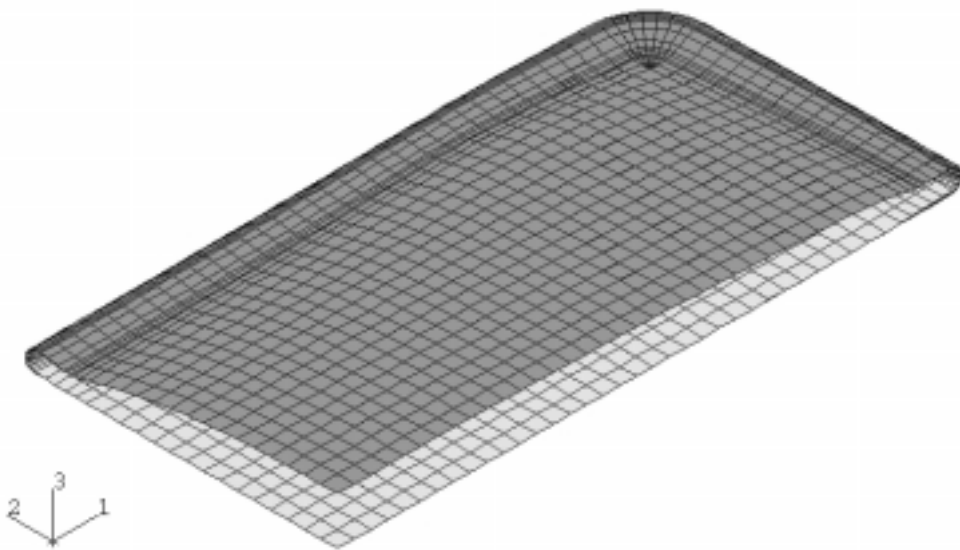


Figure 2.3.2.6: Final Shape of One-Quarter Model with "Flipped" Edges

### 2.3.3 Final Model

In the final model, the edges were modified so that they had a half-circular cross section, as shown in Figure 2.3.3.1. The radius of the half-circular cross section was 0.0215m. Due to the shape of the edges, the bottom surface of the tube was located at  $Z = 0\text{m}$ , and the top surface was located at  $Z = 0.0429\text{m}$ , with the  $Z$ -axis in the vertical direction of the tube. Assuming the tube deformation is symmetrical, only one-quarter was modeled. The center of the tube was located at  $X = 0, Y = 0$ , where the  $X$ -axis is in the longitudinal direction, and the  $Y$ -axis is in the direction of the tube's width. The origin was located at the center of the bottom surface of the tube before deformation. Boundary conditions were placed upon the nodes along the  $X$ - and  $Y$ -axes to ensure that the tube acted in a symmetrical fashion. Along the  $X$ -axis, the nodes could not move in the  $Y$ -direction nor could they rotate about the  $X$ - or  $Z$ -axes. The nodes along the  $Y$ -axis could not move in the  $X$ -direction nor could they rotate about the  $Y$ - or  $Z$ -axes.

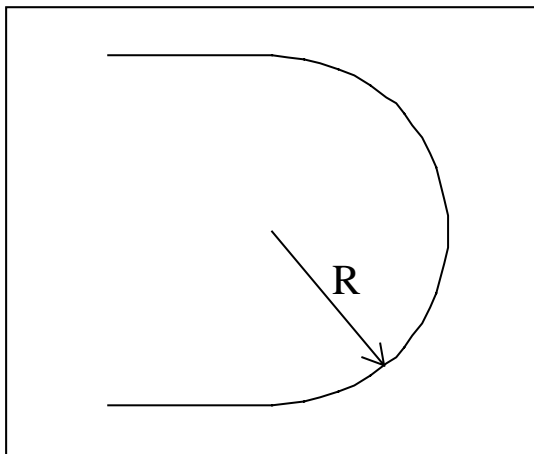


Figure 2.3.3.1: Cross Section of Edge in Final Model; Radius,  $R = 0.0215\text{m}$

The one-quarter model had one corner. It was modeled as a curved corner rather than pointed. The S3R element, degenerated from the S4R element, was used to help model the corner. The curved corner was expected to improve convergency.

Initially, 20 S4R elements were used along the half-width of both the top and bottom surfaces of the tube. Forty S4R elements were used along the half-length of both surfaces. Therefore, a total of 800 elements was used to model each quarter-surface. Twenty S4R elements were used to construct the half-circular cross-sectional edges. On the bottom surface, a tensionless spring was attached to each node, with the other end of the spring attached to the ground. Initially, each spring was modeled with a stiffness of 5700 N/m. Those springs located along the X- or Y-axis were given a spring stiffness of 2850 N/m because only one-quarter of the tube was modeled. For this same reason, the spring attached to the center node was given a spring stiffness of 1425 N/m. The initial shape of the model is shown in Figure 2.3.3.2. The edges are shown in more detail in Figure 2.3.3.3.

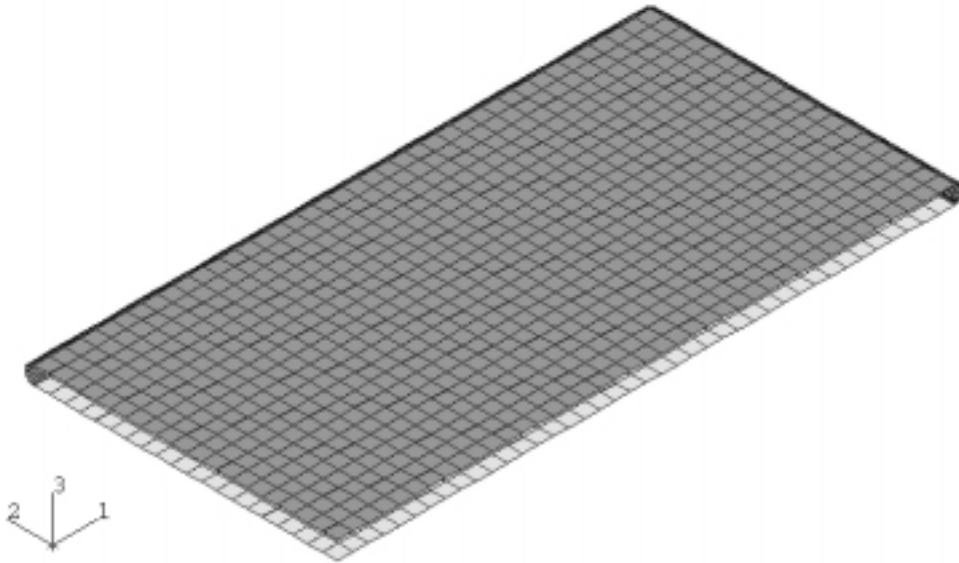


Figure 2.3.3.2: Initial Shape of Final Model Before Convergence Study

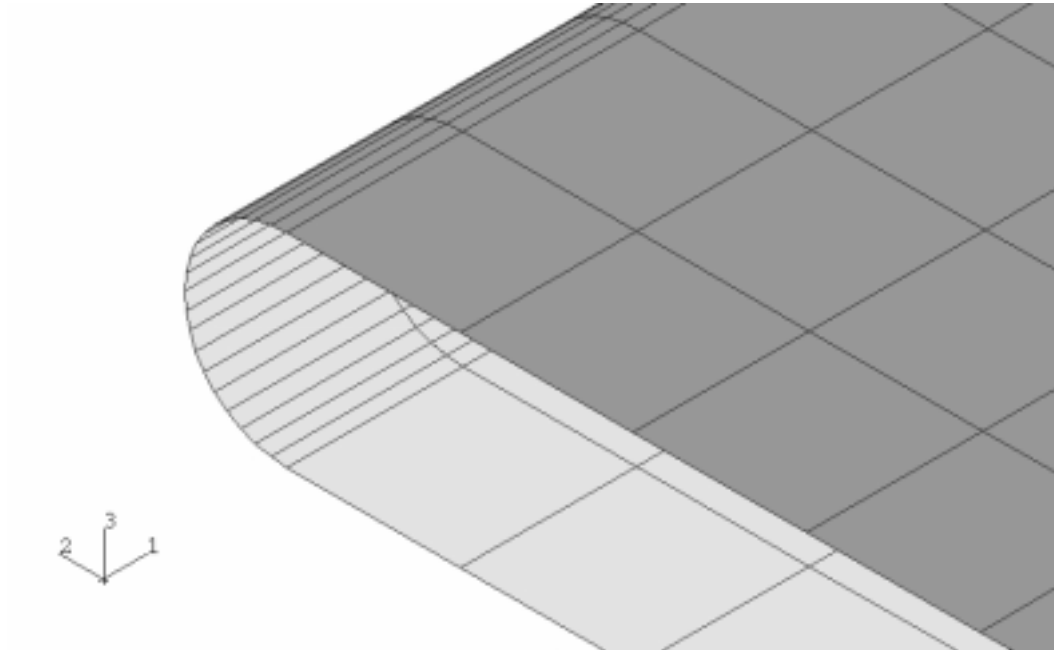


Figure 2.3.3.3: Close-Up of Edge in Final Model

## 2.4 Convergence Study

### 2.4.1 Introduction

A convergence study was then performed to determine if the mesh size of the final model provided accurate results, and whether or not the mesh should be refined or if it could be coarser to reduce the amount of CPU time during analysis.

### 2.4.2 Edges

Due to the small size of those elements which made up the top and bottom surfaces, it was expected that those surfaces would not need to be refined. Therefore, the

convergence study began with a mesh comparison at the edges. In this study, the center deflections of the top and bottom surfaces were compared, along with the mid-surface in-plane stresses  $\sigma_{11}$  and  $\sigma_{22}$  at the top surface center node. The number of elements used to make up the half-circular cross-sectional edges ranged from four to twenty. The results of the convergence study on the edges are shown in Table 2.4.2.1. As the results show, only four elements were necessary to construct the edge's half-circular cross-section.

Table 2.4.2.1: Convergence Study on Edges

# Elements at Edge	Total # Nodes	Z Top Center, m	Z Bottom Center, mm	$\sigma_{11}$ Top Center, MPa	$\sigma_{22}$ Top Center, MPa
4	1911	0.291	-1.76	12.6	1.15
8	2177	0.291	-1.76	12.6	1.14
12	2459	0.291	-1.76	12.6	1.14
16	2758	0.291	-1.76	12.6	1.14
20	3071	0.291	-1.76	12.6	1.14

### 2.4.3 Top and Bottom Surfaces

A convergence study was then performed on the top and bottom surfaces. In the study, four elements were used to construct the edge's half-circular cross-section, and the number of elements used to construct each quarter-surface ranged from 200 to 800. As the number of elements on each surface changed in the study, the stiffness of each spring changed in order to maintain a constant distributed spring stiffness. The results obtained from this convergence study are presented in Table 2.4.3.1. Based upon the results, the model which consists of 450 elements per surface provides sufficient accuracy. Therefore, the model used in this study had four elements along the half-circular cross-sectional edges, and 450 elements to form one-quarter of each surface (15 along the half-width and 30 along the half-length). Figure 2.4.3.1 depicts the initial shape of this final model.

Table 2.4.3.1: Convergence Study on the Top and Bottom Surfaces

# Elements Half-Length x Half-Width	Total # Nodes	Z Top Center, m	Z Bottom Center, mm	$\sigma_{11}$ Top Center, MPa	$\sigma_{22}$ Top Center, MPa
20 x 10	561	0.289	-1.84	12.8	1.11
30 x 15	1136	0.290	-1.79	12.6	1.14
40 x 20	1911	0.291	-1.76	12.6	1.15

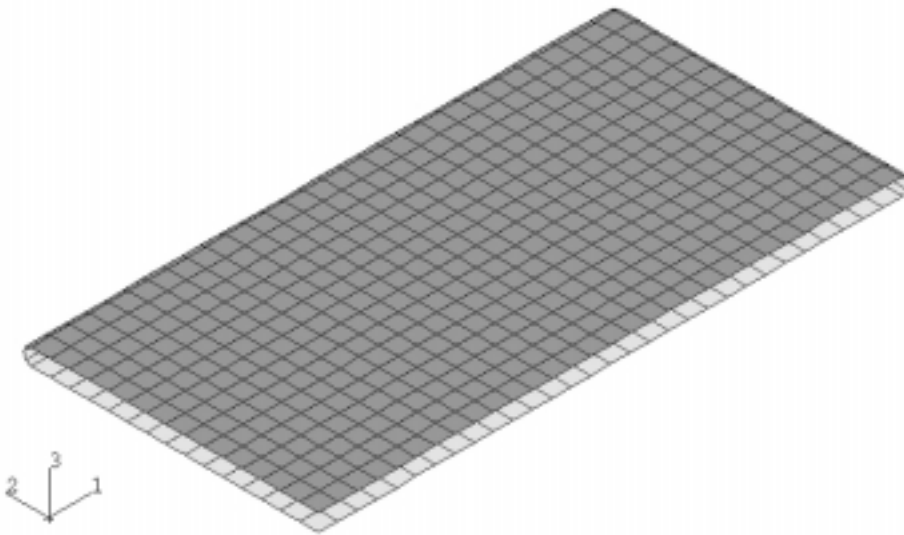


Figure 2.4.3.1: Initial Shape of Final Model After Convergence Study

## 2.5 Comparison with Celep (1988b)

A comparison was made with Celep (1988b), who performed an analytical study on a rectangular plate resting on a tensionless Winkler foundation. Celep studied the contact region between a plate and its foundation when a load is applied. One case studied was a concentrated load applied to the center of a rectangular plate with a length-to-width ratio of 2:1. This is the case used in this comparison.

Celep made several assumptions in his study. A nondimensionalized spring stiffness of  $k = 1000$  was used for the tensionless elastic foundation, and the Poisson's ratio for the plate was 0.25. A linear analysis was performed; therefore, a change in the magnitude of the loading would have no effect on the contact region. Figure 2.5.1 shows the results found in Celep's study. The x- and y-axes are nondimensionalized, with  $x = 0$  and  $y = 0$  at the center of the plate, and half of the plate is shown. The curve with  $\beta = 0.5$  represents a plate with a length-to-width ratio of 2:1.

A rectangular plate, with a length-to-width ratio of 2:1, resting on a tensionless elastic foundation, was modeled using finite element analysis. In the model,  $a = 1.5\text{m}$ ,  $b = 0.75\text{m}$ ,  $t = 0.1\text{m}$ ,  $\nu = 0.25$ , and  $E = 1.038 \times 10^8 \text{ Pa}$ . The tensionless elastic foundation was modeled using springs, with each spring having a spring stiffness  $K = 1592.29 \text{ N/m}$ ; the spring stiffness was specified in a manner such that  $K = 0$  when the spring is in tension, and  $K = 1592.29 \text{ N/m}$  when the spring is in compression. These parameters resulted in a nondimensionalized spring stiffness of  $k = 1000$  for the model, where  $k = K_d a^4 / D$ . A linear geometric analysis was performed with a concentrated load applied to the center of the plate. The resulting contact region is shown in Figure 2.5.2. The contact region agrees well with that of Celep (1988b).

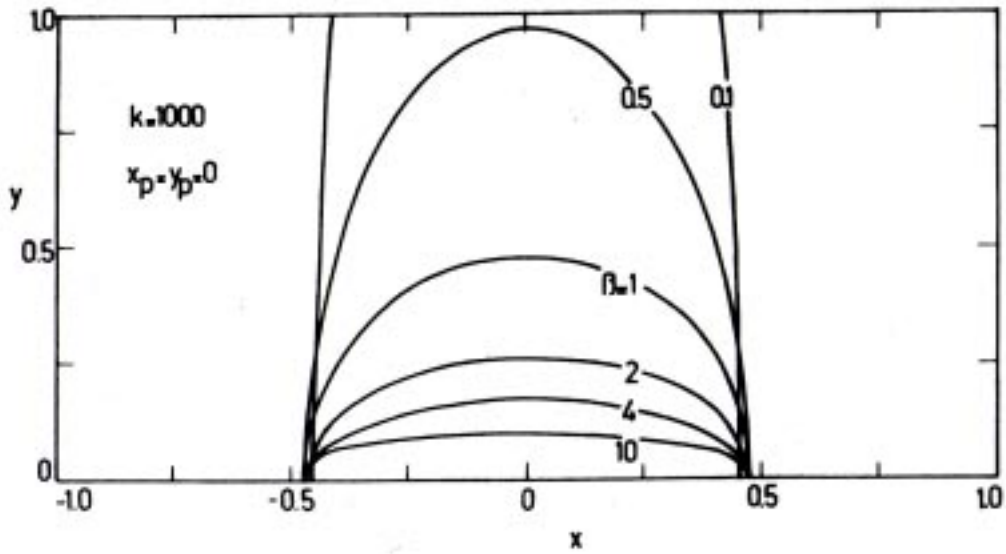


Figure 2.5.1: Contact Region Found from an Analytical Study Presented in Celep (1988b)

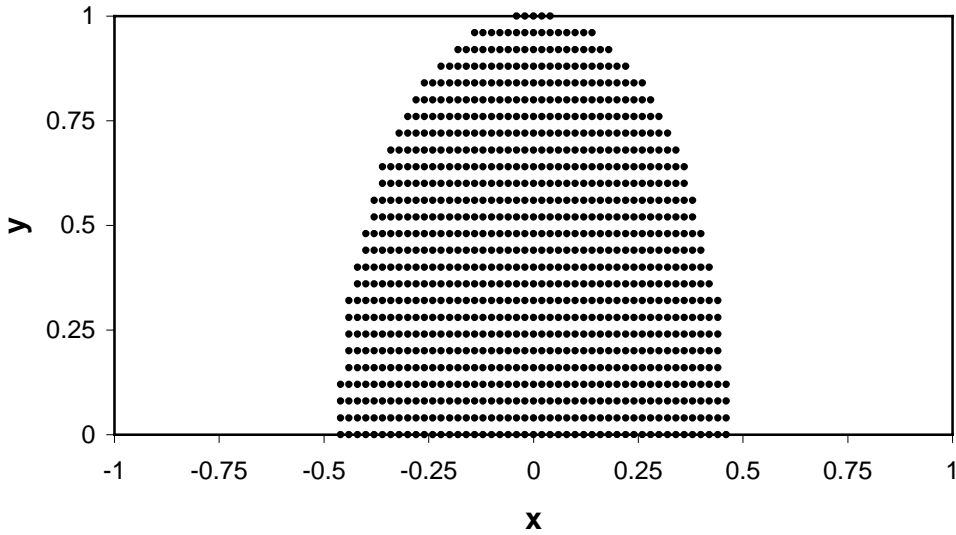


Figure 2.5.2: Contact Region Found Using Finite Element Analysis